Design Considerations of a Bearingless Motor for High-Purity Mixing Applications

B. Warberger*, T. Reichert*, T. Nussbaumer**, and J.W. Kolar*

* ETH Zurich, Power Electronic Systems Laboratory, 8092 Zurich, (*Switzerland*)
** Levitronix GmbH, 8005 Zurich, (*Switzerland*)

***Abstract* – This paper presents how a bearingless motor with exterior rotor can be implemented successfully in high-purity mixing applications. Important design parameters are identified and their influence on the system performance is demonstrated. The mechanical setup, the principle of bearing force and torque generation, the power electronics, the closed-loop control and the cooling concept are introduced in detail. Moreover, design considerations about optimizing the motor performance, the efficiency and the heat distribution are presented. Finally, the performance of the new motor is verified with a laboratory prototype.**

***Index Terms* – Bearingless motor, exterior rotor, high-purity, pharmaceutical mixing.**

I. Introduction

The bearingless slice motor was developed by R. Schoeb and N. Barletta [1,2]. This motor setup enables a contact-free suspension and propulsion of a disk-shaped rotor. Due to this unique property, the rotor can be operated in a hermetic encapsulated environment. Therefore, this totally wear- and lubrication-free motor is predestined for high-purity applications and in the last years several products, based on this bearingless motor, were successfully established on the market [3]. Today the main field of application is the semiconductor industry were the bearingless motor is used as a high-purity pump or as a wafer processing tool [4].

The pharmaceutical, the food and the chemical industry could be a new rewarding application area for the bearingless motor if appropriately implemented in high-purity mixers. The simplest mixer type is the stirred vessel [cf. Fig. 1(a)] [5,6]. There, a loop flow in the mixer tank is generated by an agitator which is connected mechanically to a motor outside the tank. A sealing and a mechanical bearing must be implemented, where the drive shaft penetrates the tank wall. The process fluid can be contaminated by wear from the mechanical bearing or by foreign particles passing through the sealing. Pinch-off areas and low-flow zones around the sealing can harm delicate fluids or can cause sedimentation, respectively. Thus, this mixer setup does not meet high-purity requirements.

In state-of-the-art mixers, magnetic couplings are used to propel the agitator [cf. Fig. 1(b)]. Thus, neither a shaft nor a sealing is needed. The torque is transmitted through the enclosed tank wall by magnetic forces and the agitator

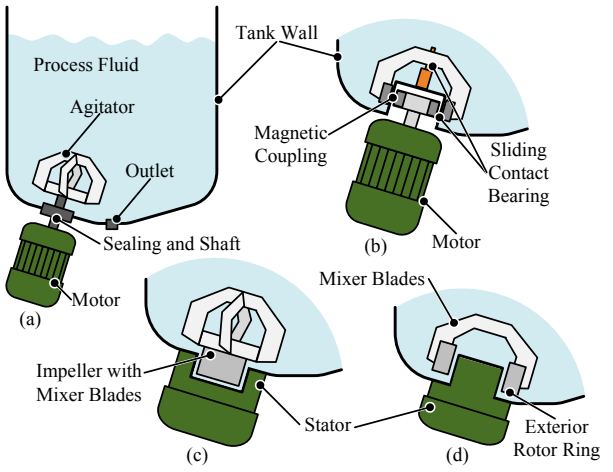

Fig. 1. Schematic view of different mixer topologies: (a) Stirred vessel with shaft and sealing, (b) mixer with sliding contact bearings and magnetic coupling, (c) bearingless interior rotor mixer and (d) bearingless exterior rotor mixer.

inside the tank is spatially seated by ceramic sliding bearings. Although the shaft and the sealing could be eliminated, the problem of small air gaps (pinch-off areas) is still existent and contact-free operation cannot be guaranteed. Moreover, the dry-running capability of the sliding bearing is very poor.

In order to meet the constantly tightened purity requirements of the aforementioned industry branches a bearingless motor topology must be implemented. Rotor suspension and torque are generated by means of magnetic forces through the tank wall. The contact-free operation and the large possible air gap eliminate wear and pinch-off areas and enable unlimited dry-running. In principle, two designs are possible – a bearingless motor with an interior rotor [cf. Fig. 1(c)] or with an exterior rotor [cf. Fig. 1(d)]. The exterior rotor design is advantageous over the interior rotor design because there is no recess in the tank wall which would cause low-flow zones and fluid residua when draining the tank. Another advantage of the bearingless mixer is that the rotor can be removed conveniently for cleaning but also clean-in-place (CIP) and sterilisation-in-place (SIP) can be applied easily [7].

In this paper various design considerations of a bearingless motor with exterior rotor for high-purity mixing applications are presented. In Section II and III the mechanical setup and performance optimizations are discussed. Section IV deals with the generation of bearing forces and torque. In Section V, VI and VII the power electronics, the sensor system and the closed-loop control

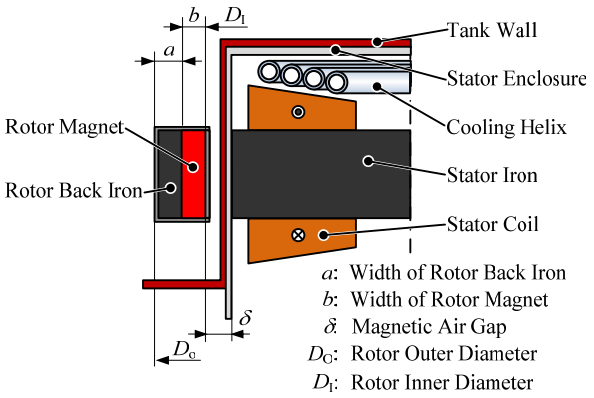

Fig. 2. Schematic view of the build-up of the bearingless motor with exterior rotor.

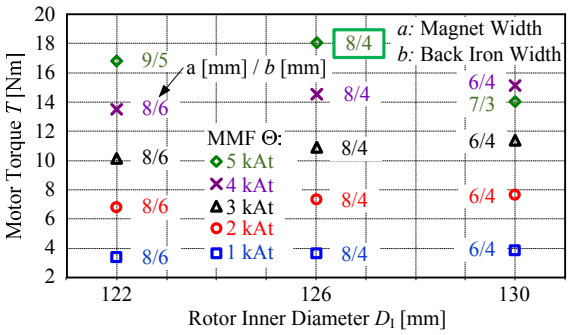

Fig. 3. Dependency between the rotor inner diameter D_I and the maximal achievable torque T for various stator excitations Θ. For each data point the optimal relation between the rotor back iron width b and the rotor magnet width a is indicated.

are presented. In section VIII a thermal model of the mixer is introduced and finally, in section IX the laboratory prototype is presented.

II. Mechanical Setup

In Fig. 2 the principle mechanical setup is depicted. The stator consists of the stator iron and the stator coils which are protected by a stator enclosure. The stator is placed outside the tank in a bay. The rotor is placed inside the tank and consists of the rotor permanent magnets and the rotor back iron. To protect the magnets and the iron form aggressive process fluids the rotor is encapsulated with stainless steel.

In order to meet the standards of manufacturers of mixing systems and to allow the usage of the bearingless motor in a targeted 2000 litre tank, the outer diameter of the exterior rotor must be limited to $D_o = 150$ mm. A magnetic air gap of $\delta = 5$ mm is required considering the thickness of the stator enclosure (1 mm), the rotor encapsulation (1 mm) and the tank wall (1 mm).

In order to enable water cooling of the stator a cooling helix is placed next to the stator windings.

III. Optimization of Motor Performance

Design consideration of the motor geometry of a bearingless motor with exterior rotor are presented in [8] in great detail. It arises that the best motor performance is achieved with six stator teeth and 16 rotor magnets. Since the outer rotor diameter D_O and the magnetic air gap δ is determined by mixer manufacturer standards the most important remaining influential degree of freedom is the inner rotor diameter D_I. With increasing D_I the lever arm for the torque generation is growing but the width of the rotor magnets a and the rotor back iron b is reduced accordingly. In Fig. 3 the dependency between the motor torque T and the inner rotor diameter D_I is depicted. It arises that with an inner rotor diameter $D_I = 126$ mm, a rotor magnet width of $a = 8$ mm and a rotor back iron width of $b = 4$ mm the maximal torque is achieved.

IV. Generation of Bearing Forces and Torque

With the proposed setup independent generation of radial bearing forces and torque is achievable. The calculation of bearing forces

$$F_{x,y} = f(N, I_{BNG}, \varphi) \tag{1}$$

and the motor torque

$$T = f(N \cdot I_{DRV}) \tag{2}$$

is described in [8] in great detail. Both, bearing forces and torque depend on the stator winding number N. I_{DRV} is the drive current (torque generation), I_{BNG} is the bearing current (radial force generation) and φ is the angular rotor position.

Fig. 4(a) and Fig. 4(b) depict an example constellation for radial bearing force generation and torque generation, respectively.

V. Winding Concept & Power Electronics

In order to operate the bearingless mixer two winding concepts are applicable. The first concept uses a drive coil with N_{DRV} turns to generate the torque and a separated bearing coil with N_{BNG} turns to generate the radial bearing forces on each stator teeth. The drive coil is energized with the mmf $\Theta_{DRV} = N_{DRV} \cdot I_{DRV}$ and the bearing coil with the mmf $\Theta_{BNG} = N_{BNG} \cdot I_{BNG}$. For a stator with six teeth twelve coils are necessary.

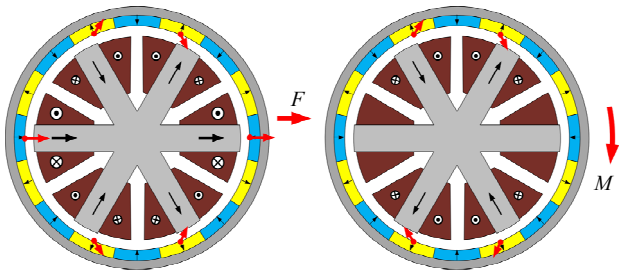

Fig. 4. Example constellation for (a) radial force and (b) torque generation.

Another concept is to install only one combined coil with $N_{combined}$ turns on each stator teeth. With the stator current I the mmf $\Theta_{combined} = N_{combined} \cdot I$ is generated.

The relation between the two winding concepts is given by the mmf Θ in the stator teeth:

$$\Theta_{combined} = \Theta_{DRV} + \Theta_{BNG} \tag{3}$$

The setup with combined windings is advantageous over the setup with two separated coils because the copper losses and the complexity of the mechanical setup can be reduced significantly [9]. A disadvantage is the higher control effort to calculate the stator current I in the combined coil.

In Fig. 5 the schematic of the power supply of the mixer motor is depicted. The DC link capacitor is fed via a three-phase bridge rectifier. In order to supply the six combined stator coils (L_1 to L_6) two commercially available three-phase half bridge modules are implemented. Always three stator coils are connected in star. The usage of these compact power modules with integrated control logic makes the power supply compact, easy to build up and low-cost.

VI. Sensor System

For the operation of the bearingless mixer motor the permanent knowledge of the radial rotor displacement (x,y) and the angular rotor position φ is essential.

Normally, the radial rotor displacement could be detected by eddy-current sensors and the angular rotor position is measured with hall-effect sensors which detect the magnetic field of the rotor magnets. In most cases the mixer tank wall is made of stainless steel. Therefore, the sensitivity of the eddy-current sensors is muted heavily and the signal-to-noise ratio is decreased dramatically. Thus, eddy-current sensors cannot be applied and another sensor system must be found.

In order to measure the radial rotor displacement through stainless steel six hall-effect sensors can be applied which are evenly distributed along the stator outline. With this sensor setup the radial rotor displacement (x,y) and the angular rotor position φ

$$(x, y, \varphi) = f(H1, H2, H3, H4, H5, H6) \tag{4}$$

can be calculated from the hall-effect sensor outputs $H1$ to $H6$.

When examining the performance of this system, it arises that the position measurement is affected by the stator currents because the hall-effect sensors measure not only the field of the permanent magnets but also the magnetic stray field generated by the stator coils. Since the stator currents are measured for the closed-loop control this effect can be compensated mathematically.

Another problem is the varying magnetization of the permanent magnets. In order to compensate these manufacturing tolerances a calibration routine must be implemented. In a first step the remanence flux density of the magnets is measured and stored in a look-up table. Then, during operation, the gain of each sensor is adjusted accordingly to compensate the tolerances.

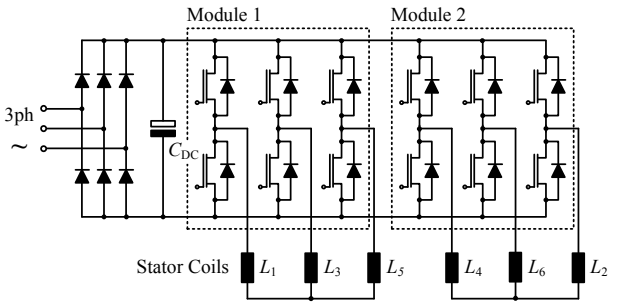

Fig. 5. Simplified schematic of the implemented power electronics. The DC link capacitor is fed by a three-phase rectifier bridge. The six stator coils of the motor are connected in star and are powered by two three phase-half bridge modules.

VII. Closed-Loop Control

The control mechanism of the bearingless mixer motor is similar to the field oriented control of a permanent magnet synchronous motor. Only a position control system must be added, due to the magnetic suspension of the rotor. In Fig. 6 a schematic overview of the closed-loop control is depicted. Two subsystems can be identified – the speed control and the position control.

The speed controller compares the actual speed with the speed set point and outputs the reference drive current ($i_{DRV,ref}$) for the drive current controller. The latter compares the reference with the measured drive current ($i_{DRV,meas}$) and sets the drive duty cycle (D_{DRV}).

A similar system is applied in the position control loop. The reference rotor position ($\underline{\boldsymbol{x}}_{ref}$, normally centred to the stator) is compared with the measured position ($\underline{\boldsymbol{x}}$) and the reference bearing currents ($\underline{\boldsymbol{i}}_{BGN,ref}$) are calculated accordingly by the PID position controller. (A derivative component must be added to the position controller in order to stabilize the innately instable magnetic plant.) The reference bearing currents are compared with the actual bearing currents ($\underline{\boldsymbol{i}}_{BNG,meas}$) and appropriate bearing duty cycles ($\underline{\boldsymbol{D}}_{BNG}$) are set by the bearing current controller.

All these aforementioned calculations take place in a rotor fix reference frame. Therefore, the calculated duty cycles for the drive and bearing currents must be transformed into the stator fix three-phase reference frame (Park transformation). Moreover, due to the combined coils (see section V) also a superposition of the drive and bearing duty cycles for each stator coil must occur. This superposition and the Park transformation are combined in the transformation $\boldsymbol{T}^{-1}(\varphi)$. With the reverse transformation $\boldsymbol{T}(\varphi)$ the measured stator currents are spitted up into the drive and bearing part and are projected onto the rotor fix reference frame.

VIII. Thermal Model

The winding number of the stator coils is limited by the stator volume and in order to achieve high torque high stator currents must be impressed. Therefore, the temperature development inside the stator must be investigated. This can be done by a finite element simulation.

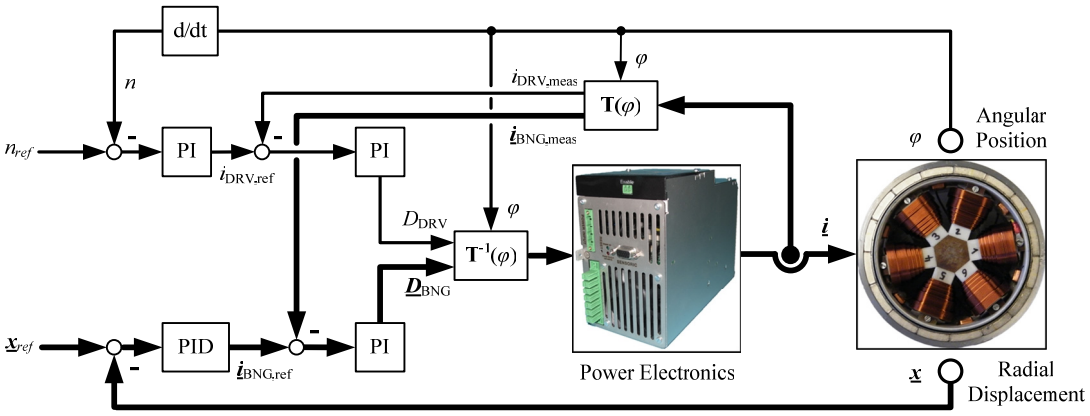

Fig. 6. Schematic overview of the closed-loop control of the bearingless mixer motor with exterior rotor. The signal paths of multidimensional variables are plotted bolt. [n_{ref}: reference speed, n: actual speed, $\underline{x}_{ref}$: reference rotor position, $\underline{x}$: actual rotor position, $i_{DRV,ref}$: reference drive current (torque generation), $\underline{i}_{DRV,meas}$: actual drive current, D_{DRV}: duty cycle for drive current, $\underline{i}_{BNG,ref}$: reference bearing currents (radial forces generation), $i_{BNG,meas}$: actual bearing currents, $\underline{D}_{BNG}$: duty cycles for bearing currents, $\underline{i}$: actual stator currents and φ: angular rotor position.]

However, this is computationally intensive and can take several hours. In order to quickly check the influence of some design parameters on the temperature distribution an analytical thermal model was set up. In Fig. 7 an exemplary equivalent electric network of the proposed thermal model is depicted. Heat sources (e.g. copper losses) are modelled as current sources and points of constant temperature (e.g. temperature of mixer fluid and cooling helix) are modelled as voltage sources. The thermal resistances can be calculated with the knowledge of the dimensions and thermal conductivity of the corresponding mixer components [10]. Once the equivalent electric network is set up, the temperatures in the mixer can be gained quickly by solving a set of linear equations.

Two important questions must be answered with the thermal model. First, is an additional cooling system necessary when running the mixer with full load (20 Nm) or is the cooling effect of the surrounding mixer fluid sufficient? Secondly, can an internal component (especially the sensor electronic) be damaged when the mixer tank is sterilized at a temperature of 130 °C?

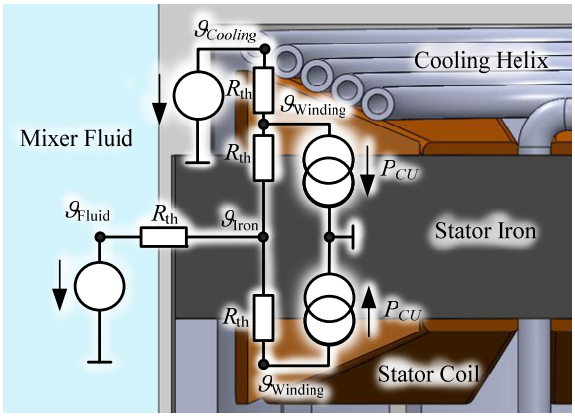

Fig. 7. Exemplary equivalent electric network for the analytic thermal model.

In Fig. 8 the results of the thermal simulation are depicted. In Fig. 8(a) the mixer is operating with 20 Nm without an additional cooling system and in Fig. 8(b) internal water cooling is applied. It arises that the additional cooling system is essential and the hot spot (winding temperature) could be reduced form 220 °C to approx. 100 °C. In Fig. 8(c) the temperature distribution during the sterilization process without water cooling is depicted, whereas in Fig. 8(d) water cooling is applied. Again, the temperatures of the mixer interior could be reduced significantly by the additional cooling system but also without water cooling the mixer would not take damage during the short sterilisation process.

The applied materials also have a significant influence on the temperature distribution. The most important factor is the thermal conductivity u of the pottant. In Fig. 9 the dependency between the interior motor temperature and the applied torque for two different pottants is depicted. The use of a pottant with a thermal conductivity of more than $u > 1$ W/(m·K) is not recommendable because pottants with higher thermal conductivity u exhibit a too large thermal expansion.

IX. Experimental Setup

In order to verify the aforementioned design considerations a laboratory prototype of the bearingless mixer motor with exterior rotor was set up (cf. Fig. 10).

First, the robustness of levitation of the exterior rotor was investigated. Therefore, the system response to a radial position step of the rotor was recorded. Due to the restraining effect of a mixer fluid this test was conducted in air in order to simulate a worst case scenario. In Fig. 11(a) the system response is depicted when an x-axis offset of 0.25 mm is added to the reference position of the rotor. It arises that the rotor can be placed stable at any position within the mechanical air gap of 2 mm.

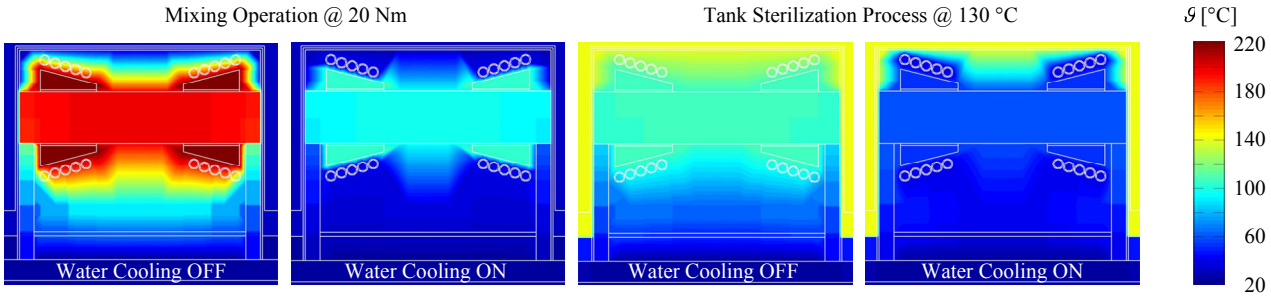

Fig. 8. Temperature distribution in the mixer cross section at various operation points. In (a) the temperature in the stator at a torque of 20 Nm without water cooling is shown. If water cooling is applied (b) the temperature during operation declines significantly. In (c) the sterilisation of the tank with steam (130 °C) and without water cooling is simulated, whereas (d) shows the same process but with activated water cooling. For all simulations an ambient temperature of 24 °C and a cooling water temperature of 40 °C were assumed. The temperature of the process fluid inside the tank was assumed to be 30 °C. Water cooling was realized by a cooling helix directly above and below the stator coils.

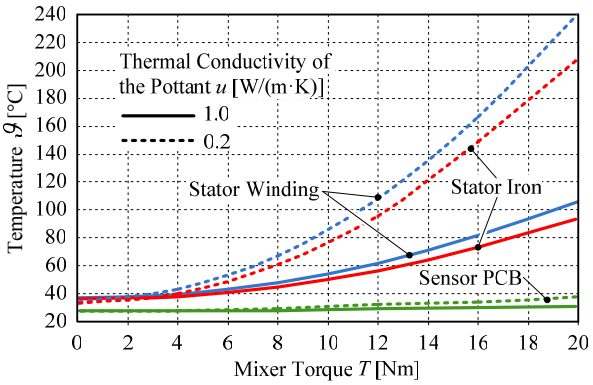

Fig. 9. Simulated influence of torque T and thermal conductivity u of the pottant on the temperature ϑ of stator winding, stator iron and sensor pcb. The pottant has a significant impact on the temperature.

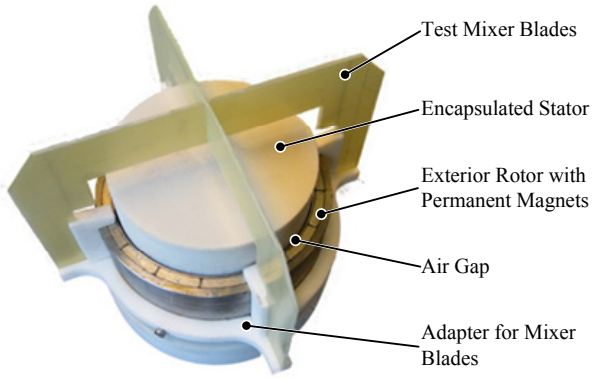

Fig. 10. Experimental mixer motor setup. Outer diameter of the encapsulated stator is 120 mm and outer rotor diameter is 150 mm. The mechanical air gap is 2 mm. For test purpose test mixer blades have been mounted.

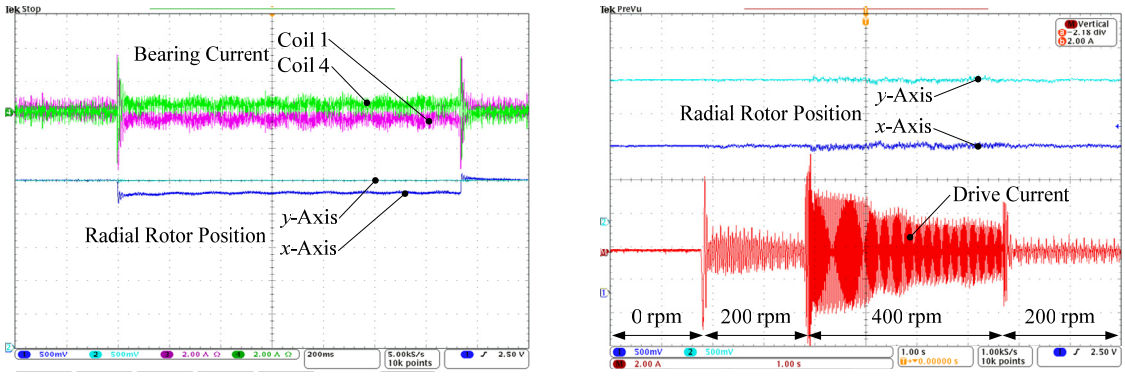

Fig. 11. Verification of the performance of the bearingless motor: In (a) the system response to a radial reference step from $x = 0$ mm to $x = 0.25$ mm is depicted. Since the drive was disabled the coil current is equal to the bearing current. Coil 1 and Coil 4 are placed along the x-axis. The test was conducted in air (current scale 2 A/div, radial position scale 0.5 mm/div and time scale 200 ms/div). In (b) the radial position and the drive current in dependency of the rotor speed is depicted. The motor was operated in water (current scale 2 A/div, radial position scale 0.5 mm/div and time scale 1 s/div).

In a next step, the bearingless motor was tested in water. In Fig. 11(b) the performance at various speeds is depicted. This test reveals that the mixer can operate up to the targeted speed of 500 rpm. Despite of the fluid forces acting on the rotor the magnetic bearing is able to provide contact-free operation over the whole speed range.

X. Conclusion

In this paper design considerations concerning a bearingless mixer motor with exterior rotor were presented. Important principles and problems concerning the mechanical setup, performance optimization, the generation of bearing forces and torque, the power

electronics, the sensor system, the closed-loop control and the thermal model of the motor have been discussed in detail. Finally, a laboratory prototype was built up and tested in water. With extensive performance tests the applicability of this innovative motor concept could be demonstrated.

REFERENCES

[1] R. Schoeb and N. Barletta, "Principle and Application of a Bearingless Slice Motor" in *JSME international journal. Series C, Mechanical systems, machine elements and manufacturing*, vol. 40, pp. 593-598, 1997.

[2] S. Silber, W. Amrhein, P. Bösch, R. Schoeb, N. Barletta, "Design aspects of bearingless slice motors", in *IEEE/ASME Transaction on. Mechatronics*, vol. 10, no. 6, pp. 611-617, Dec. 2005.

[3] Levitronix GmbH: www.levitronix.com.

[4] T. Schneeberger, T. Nussbaumer, J. W. Kolar, "Magnetically Levitated Homopolar Hollow-Shaft Motor", in *IEEE/ASME Trans. Mechatronics*, vol. 15. pp. 97-107, 2010.

[5] E. Paul, V. Atiemo-Obeng and S. Kresta, "Handbook of Industrial Mixing", John Wiley & Sons, Inc., New Jersey, 2004.

[6] J. A. Asenjo and J. C. Merchuk, "Bioreactor System Design*"*, Marcel Dekker, Inc., New York, 1995.

[7] Y. Christi and M. Moo-Young, "Clean-in-place systems for industrial bioreactors: Design, validation and operation", in *Journal of Industrial Microbiology and Biotechnology,* vol. 13, pp. 201-207, July 1994.

[8] T. Reichert, T. Nussbaumer, J. W. Kolar, "Novel Bearingless Brushless Motor in Exterior Rotor Construction for Stirred Bioreactors", *PEMD10*, Brighton, UK, April 2010.

[9] K. Raggl, T. Nussbaumer, J. W. Kolar, "Comparison of Separated and Combined Winding Concepts for Bearingless Centrifugal Pumps", in *Journal of Power Electronics*, vol. 9, no. 2, pp.243-258, 2009.

[10] J. H. Lienhard IV, J.H. Lienhard V, "A Heat Transfer Textbook", 3rd ed., Cambridge, MA: Phlogiston Press, 2004.